A 3D-Var Assimilation Scheme for Vertical Velocity with the CMA-MESO v5.0

Hong Li[1,2], Yi Yang[1], Jian Sun[3], Yuan Jiang[3], Ruhui Gan[1], Qian Xie[1]

[1]Key Laboratory of Climate Resource Development and Disaster Prevention in Gansu Province, Center for Weather Forecasting and Climate Prediction of Lanzhou University, College of Atmospheric Sciences, Lanzhou University, Lanzhou 730000, China
[2]Institute of Arid Meteorology, China Meteorological Administration, Lanzhou 730020, China
[3]China Meteorological Administration Earth System Modeling and Prediction Centre, Beijing 100081, China

Correspondence to: Yi Yang (yangyi@lzu.edu.cn)

Abstract. Certain vertical motions associated with meso-microscale systems are favorable for convection development and maintenance, correct initialization of updraft motions is thus significant in convective precipitation forecasts. A three-dimensional variational-based vertical velocity (w) assimilation scheme has been developed within the high-resolution (3 km) CMA-MESO (the Mesoscale Weather Numerical Forecast System of China Meteorological Administration) model. This scheme utilizes the adiabatic Richardson equation as the observation operator for w, enabling the update of horizontal winds and mass fields of the model's background. The tangent linear and adjoint operators are subsequently developed and undergo an accuracy check. A single-point w observation assimilation experiment reveals that the observational information is effectively spread both horizontally and vertically. Specifically, the assimilation of w contributes to the generation of horizontal wind convergence at lower model levels and divergence at higher model levels, thereby adjusting the locations of convection occurrence. The impact of assimilating w on the forecast is then examined through a 10-day continuous run. The further assimilation of w, in addition to the conventional and radial wind data assimilation, significantly improves the positional forecast accuracy of precipitation, resulting in higher FSS (frequency skill score) values. Additionally, the assimilation of w demonstrates improved performance in predicting hourly precipitation at higher thresholds (5 and 20 mm h^{-1}), as indicated by higher ETS (equitable threat score) skills. However, it should be noted that further assimilation of w can potentially lead to some false precipitation, resulting in slightly lower ETS values at lower thresholds (1 mm h^{-1}) and a neutral impact on BIAS (bias score) skills. An individual case study conducted within the batch experiments reveals that assimilating w has a beneficial impact on the enhancement of vertical motion across different layers of the model, facilitating the transport of moisture from lower to mid-high model levels, thereby leading to an improvement in forecast skills.

1 Introduction

The vertical component of atmospheric motion plays a pivotal role in defining convection, as it directly influences the formation and development of clouds along with their associated precipitation. In numerical models, vertical motions are of

utmost importance in parameterizing cloud dynamics and microphysical processes. This significance stems from their ability to describe the coupling between atmospheric dynamics and cloud formation and development. Consequently, they hold a crucial position in forecasting convective-scale precipitation (see, e.g., Donner et al., 2001; Lang et al., 2007; Panosetti et al., 2019; Tao et al., 2022). A three-dimensional analysis field that accurately involves both updrafts and downdrafts holds significant promise in enhancing the forecast accuracy of convective precipitation.

The vertical velocity (w) is difficult to measure directly or estimate due to its transient nature and relatively small magnitude, which is typically a few orders of magnitude smaller than the mesoscale horizontal velocities (Lee et al., 2003; Tarry et al., 2022). The well-known direct measurement is the research aircraft (e.g., LeMone and Zipser. 1980; Houze and Betts 1981; Rodts et al., 2003; Anderson et al., 2005; May et al., 2008; Heymsfield et al., 2010) but with limited spatial and temporal coverage. Besides, the nature of vertical velocities allows them can be inferred from balanced dynamics. The widely acknowledged inference of such is the so-called "continue equation", from which the w pseudo-observations are derived from horizontal divergence or convergence (Bellamy 1949; Cifelli et al., 1996). Based on the above principle or other algorithms (e.g., Williams, 2012), the w values can also be retrieved from remote sensing instruments, such as wind profilers and scanning Doppler radars (e.g., Lee et al., 2003; Liu et al., 2005; Lee et al., 2006; Heymsfield et al., 2010; Giangrande et al., 2013; Ovchinnikov et al., 2019). Motivated by the development of observation instruments and inversion algorithms, more and more updrafts and downdrafts velocity "observations" emerged, especially at the cloud-resolve scale (e.g., Doppler radar and lightning data), so it is necessary to evaluate the effects of w assimilation on convective-scale precipitation forecasting.

In fact, efforts have been made to assimilate dynamic information associated with atmospheric vertical motions in recent research. For example, the w information retrieved from lightning data was assimilated based on the well-defined correlation (Price and Rind, 1992) between the total lightning flash rate and the updraft velocities (Wang et al., 2020; Xiao et al., 2021; Gan et al., 2021). These studies have shown that the assimilation of w improves the water vapor and dynamic fields, and thus produces better convective precipitation forecasts. It should be noted that another work by Gan et al. (2022) revealed that the assimilation of the "zero" column maximum w can also effectively suppress spurious convections by weakening vertical motions and reducing the hydrometeors and humidity of the model. The above w assimilation attempts are based on the nudging (Wang et al., 2020), four-dimensional variational (Xiao et al., 2021), or ensemble square root filter (Gan et al., 2021, 2022) methods, which are 1) relatively difficult to apply into the operational mesoscale regional model for computational cost consideration or 2) lack of strict physical constraints.

Since the three-dimensional variational (3D-Var) method is still widely used in operations (Gustafsson et al. 2018) due to its lower computation costs and its ability to assimilate nonmodal variables, the development of a 3D-Var assimilation technique for w observation becomes necessary. Within the 3D-Var framework, assimilating w faces numerous difficulties, the most challenging of which is the establishment of an effective assimilation method that produces a reasonable positive impact on forecasts. By extending w as a control variable, direct assimilation of w becomes feasible, simplifying the observation operator into a mapping algorithm from model space to observation space. However, as noted by Chen et al.

(2020), the imbalance between microphysical and dynamic fields may lead to excessive noise when directly assimilating w observations as a control variable, accomplished by adding an observation term to the 3D-Var cost function. To address this issue, Chen et al. (2020) initially computed horizontal convergence (based on the mass-continuity equation) from w pseudo-observations derived from total lightning data. Subsequently, an observation operator for horizontal convergence was developed. To achieve the direct assimilation of w while mitigating noise, a transformation observation operator, often referred to as the observation operator, is required. This operator ensures adherence to physical constraints and aims to combine the w variable and control variables for minimizing the 3D-Var cost function. In this study, the adiabatic Richardson equation (Richardson, 1922) is employed as the observation operator of w. This choice enables the simultaneous update of dynamical and mass fields, thereby promoting a more balanced final analysis. Additionally, this direct assimilation scheme avoids the inversion errors associated with an indirect assimilation approach.

In this study, a 3D-Var assimilation scheme for w is established within the Mesoscale Weather Numerical Forecast System of China Meteorological Administration (CMA-MESO) model. The following is the outline of this study: A brief description of the basic formulation of 3D-Var and the assimilation strategy for w observation is presented in Sect. 2. In Sect. 3, a single-point observation experiment is performed to test the spread of observational information of the assimilation scheme. The effect of assimilating w observations is then assessed by a 10-day continuous run and an individual case within it, and the results are presented and discussed in Sect. 4. Finally, the main conclusions are addressed in Sect. 5.

2 Assimilation system and vertical velocity assimilation strategy

2.1 CMA-MESO 3D-Var system

In this study, the CMA-MESO model version 5.0 is used as the forecast model. CMA-MESO (Shen et al., 2020) is a nonhydrostatic regional mesoscale system with a horizontal resolution of 3 km. The w assimilation scheme is constructed within the 3D-Var framework of the CMA-MESO model. In the traditional framework of a variational assimilation system, the best analysis x can be derived from c_v (the control variables including the zonal and meridional winds, pseudo-relative humidity, temperature, and surface pressure) by minimizing a cost function J of c_v (Courtier et al., 1994):

$$J(c_v) = \frac{1}{2} c_v{}^{\mathrm{T}} c_v + \frac{1}{2} (\mathbf{H}\mathbf{U}c_v + d)^{\mathrm{T}} \boldsymbol{R}^{-1} (\mathbf{H}\mathbf{U}c_v + d), \quad (1)$$

$$x = x^b + \mathbf{U}c_v, \quad (2)$$

where x^b is the background, $\boldsymbol{R}$ is the observation error covariance, d is defined as $H(x^b)$-y^o (H denotes the observation operator and y^o is the observation), $\mathbf{H}$ is the linearized observation operator, $\mathbf{U}$ is associated with the background error covariance $\boldsymbol{B}$: $\boldsymbol{B}=\mathbf{U}^{\mathrm{T}}\mathbf{U}$. The matrix $\boldsymbol{B}$ is statistically based on National Meteorological Center method.

2.2 Observation operator for vertical velocity

The observation operator H is used to derive the model equivalent of the observations from the model state variables (Kalnay, 2002). In this study, the adiabatic Richardson equation (Richardson, 1922) is used as the observation operator:

$$\gamma P\frac{\partial w}{\partial z} = -\gamma P\nabla\cdot V_h - V_h\cdot\nabla P + g\int_z^\infty \nabla\cdot(\rho V_h)dz, \quad (3)$$

where γ is the ratio of specific heat capacities of air at a constant pressure (c_p) and at a constant volume (c_v), P is pressure, z is the height, V_h is the horizontal winds (components u and v), g is acceleration due to gravity and ρ is density. The Richardson equation combines the continuity equation, adiabatic equations, and hydrostatic relation, which enables the 3D-Var method to adjust the dynamic and mass fields simultaneously and result in a more balanced analysis field. As the terrain-following vertical coordinate (Gal-Chen and Somerville, 1975) used in the CMA-MESO model is expressed as:

$$\hat{z} = z_T\frac{z-Z_s(x,y)}{Z_T-Z_s(x,y)}, \quad (4)$$

here, z_T is the top height of the model upper boundary and z_s is the topographic height, the Eq. (3) in the terrain-following vertical coordinate can be expressed as:

$$\gamma\Pi^\kappa\frac{\Delta Z_s}{Z_T}\frac{\partial\widehat{w}}{\partial z} = -\left(u\frac{\partial\Pi^\kappa}{\partial x}+v\frac{\partial\Pi^\kappa}{\partial y}\right)+\frac{\Delta Z_z}{\Delta Z_s}\left(\frac{\partial Z_s}{\partial x}+\frac{\partial Z_s}{\partial y}\right)\frac{\partial\Pi^\kappa}{\partial z}-\gamma\Pi^\kappa\left(\frac{\partial u}{\partial x}+\frac{\partial v}{\partial y}\right)-\gamma\Pi^\kappa\frac{\partial}{\partial z}\left(\frac{\Delta Z_z}{\Delta Z_s}\right)\left(u\frac{\partial Z_s}{\partial x}+v\frac{\partial Z_s}{\partial y}\right)-\int_z^\infty\frac{\partial\Pi^\kappa}{\partial z}\left(\frac{\partial u}{\partial x}+\frac{\partial v}{\partial y}\right)dz-$$
$$\int_z^\infty\left(u\frac{\partial}{\partial x}\left(\frac{\partial\Pi^\kappa}{\partial z}\right)+v\frac{\partial}{\partial y}\left(\frac{\partial\Pi^\kappa}{\partial z}\right)\right)dz+\int_z^\infty\frac{\Delta Z_z}{\Delta Z_s}\frac{\partial\Pi^\kappa}{\partial z}\left(\frac{\partial Z_s}{\partial x}\frac{\partial u}{\partial z}+\frac{\partial Z_s}{\partial y}\frac{\partial v}{\partial z}\right)dz+\int_z^\infty\frac{\Delta Z_z}{\Delta Z_s}\frac{\partial}{\partial z}\left(\frac{\partial\Pi^\kappa}{\partial z}\right)\left(u\frac{\partial Z_s}{\partial x}+v\frac{\partial Z_s}{\partial y}\right)dz, \quad (5)$$

where u and v are the zonal and meridian wind components. Π is the dimensionless pressure, and $\Pi = \left(\frac{P}{P_0}\right)^{R/c_p}$, $P_0 = 1000$ hPa, and R is the gas constant. $\kappa = {c_p}/{R}$. ΔZ_s and ΔZ_z in Eq. (5) are defined as follows:

$$\Delta Z_s = Z_T - Z_s(x,y), \quad (6)$$

$$\Delta Z_z = Z_T - z(x,y), \quad (7)$$

$\widehat{w}$ in Eq. (5) is the w under the terrain-following vertical coordinate and is expressed as:

$$\widehat{w} = \frac{d\hat{z}}{dt} = \frac{Z_T}{\Delta Z_s}\left(w-\frac{\Delta Z_z}{\Delta Z_s}w_s\right), \quad (8)$$

where w_s is the w value at the surface and $w_s = u\frac{\partial Z_s}{\partial x}+v\frac{\partial Z_s}{\partial y}$.

The observation operator links the w variable to the u, v, and Π variables. u and v are control variables, and Π is related to the surface pressure (control variable). Thus, as the w assimilated through the Eq. (5), the w of the initial field is not updated directly, but the horizontal winds and pressure fields are updated. Since the w observation term is added as a new kind of observation to the cost function of the 3D-Var system within the CMA-MESO model, modifications made to the existing 3D-Var system include the following: 1) the observation operator for w is established to calculate observation innovation; 2) the tangent linear of the observation operator and its adjoint for the w term are included to calculate the cost function and its gradient values.

2.3 Accuracy check

After completion of the w observation operator, the correctness of the adjoint operator should be checked. For the tangent linear $\mathbf{H}$ and its adjoint $\mathbf{H}^{\mathrm{T}}$ of an observation operator, the following formula is always satisfied:

$$< \mathbf{H}(\delta x), \mathbf{H}(\delta x) >=< \mathbf{H}^{\mathrm{T}}\big(\mathbf{H}(\delta x)\big), \delta x >, \quad (9)$$

where δx represents a small perturbation and < > stands for the inner product of the vectors. The test result shows that term $< \mathbf{H}(\delta x), \mathbf{H}(\delta x) >$ is equal to 0.100159014620902D-17 (D: double precision), term $< \mathbf{H}^{\mathrm{T}}\big(\mathbf{H}(\delta x)\big), \delta x >$ is equal to 0.100159014620902D-17, and the difference between the two terms is 0.577778983316171D-33. As a result, the adjoint test has successfully passed under double precision.

For a tangent linear operator, it is also necessary to verify the correctness of the gradient using the following standard:

$$\Phi(\alpha) = \frac{J(c_v+\alpha)-J(c_v)}{\alpha \nabla J(c_v)}, \quad (10)$$

where ∇J is the gradient of J. The symbol α indicates a small value closer to zero, and the value of $\Phi(\alpha)$ is expected to be near 1. The results are presented in Table 1, showing that the tangent linear equation is accurate within the rounding error of the computer.

Table 1. Verification of gradient correctness: values of $\Phi(\alpha)$ for different α values (symbols defined in Eq. (10)).

α	$\Phi(\alpha)$
10^{-4}	1.00000684582308
10^{-5}	1.00000068454433
10^{-6}	1.00000006939151
10^{-7}	1.00000000569911
10^{-8}	1.00000003421803
10^{-9}	1.00000055706492
10^{-10}	1.00000626084813
10^{-11}	1.00001576715311
10^{-12}	1.00053861393468
10^{-13}	0.998162037654562

3 Single-point observation experiment

To investigate the spatial propagation of pseudo-observation information for variable w, a single w pseudo-observation is assimilated to assess the changes in various variables. This pseudo-observation of w is positioned at an altitude of 5448.6 m (23th model level, approximately 500 hPa) at coordinates (38.0° N, 115.2° E) (depicted as solid white or black dots in Fig. 1)

with a value of 1 m s^{-1}. The observation error is set to 0.5 m s^{-1}. The background field's w value at this location is -0.04 m s^{-1}, resulting in an innovation (observation minus background) of approximately 1.04 m s^{-1}.

The analysis increment induced by this observation is depicted in Fig. 1. The computed analysis increments of the horizontal wind field and its convergence at the 13th (~850 hPa) or 27th (~400 hPa) model level exhibit an isotropic structure centered around the observation site. Since a positive w value is assimilated, a horizontal wind convergence increment is observed at the lower (13th) model level, while a horizontal wind divergence increment occurs at the middle (27th) model level. As the w observation operator is not directly linked to temperature and specific humidity but is instead related to dimensionless air pressure, adjustments to temperature and humidity are achieved through weak physical constraints, resulting in relatively small increments in temperature and specific humidity. From the vertical cross-section of the analysis increment for each variable (Fig. 2), it can be seen that the increase in specific humidity is primarily concentrated in the lower layer below the observation location, while the increases in the other three variables are distributed throughout the entire layer. Regarding the increase in horizontal wind u, below the single point observation, there is a convergence of u wind that extends to the ground. Above the single point observation, there is a divergence of u wind that extends to approximately 150 hPa.

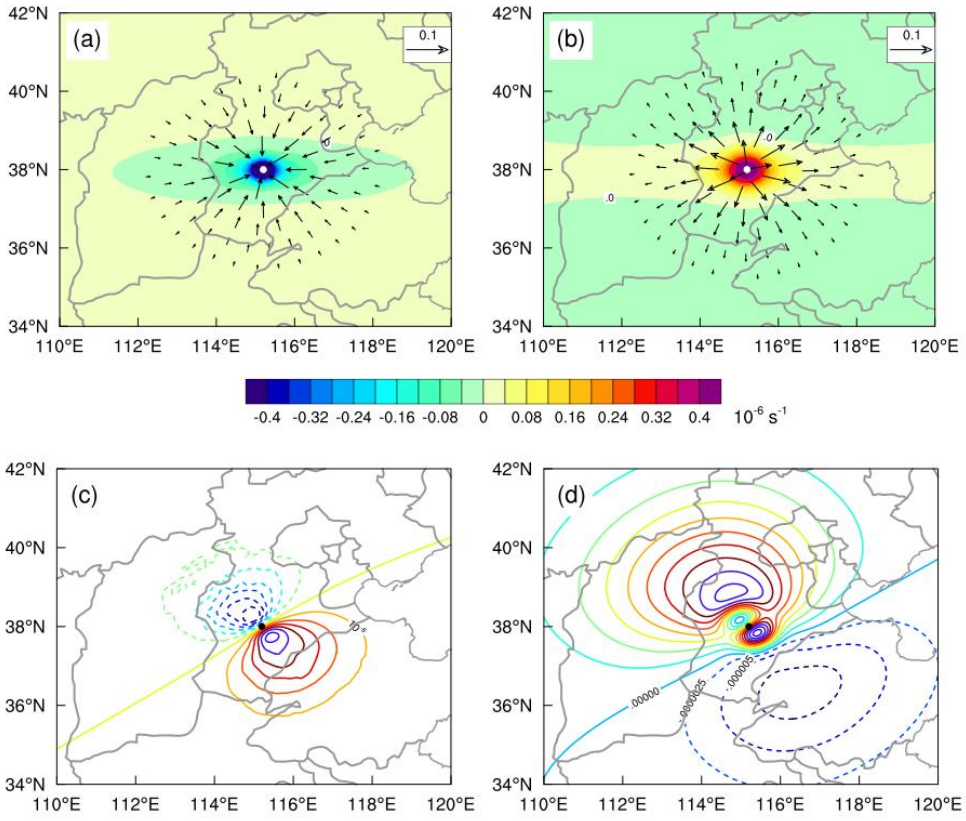

Figure 1: Analysis increments of different variables at 1500 UTC on July 4, 2020, for the single observation experiment. (a) Horizontal wind (vector; only values greater than 0.01 are shown; unit: m s^{-1}) and horizontal wind divergence (color; unit: 10^{-6} s^{-1}) increments at the 13th (~850 hPa) level of the model; (b) is the same as (a) but for the 27th (~400 hPa) level of the model. (c)

Specific humidity (interval is 10^{-8}; unit: kg kg^{-1}) and (d) temperature (interval is 2.5×10^{-6} K) increments at the 13th level of the model. The solid white (black) dots in (a) and (b) ((c) and (d)) indicate the locations of the single w observation (38.0° N, 115.2° E).

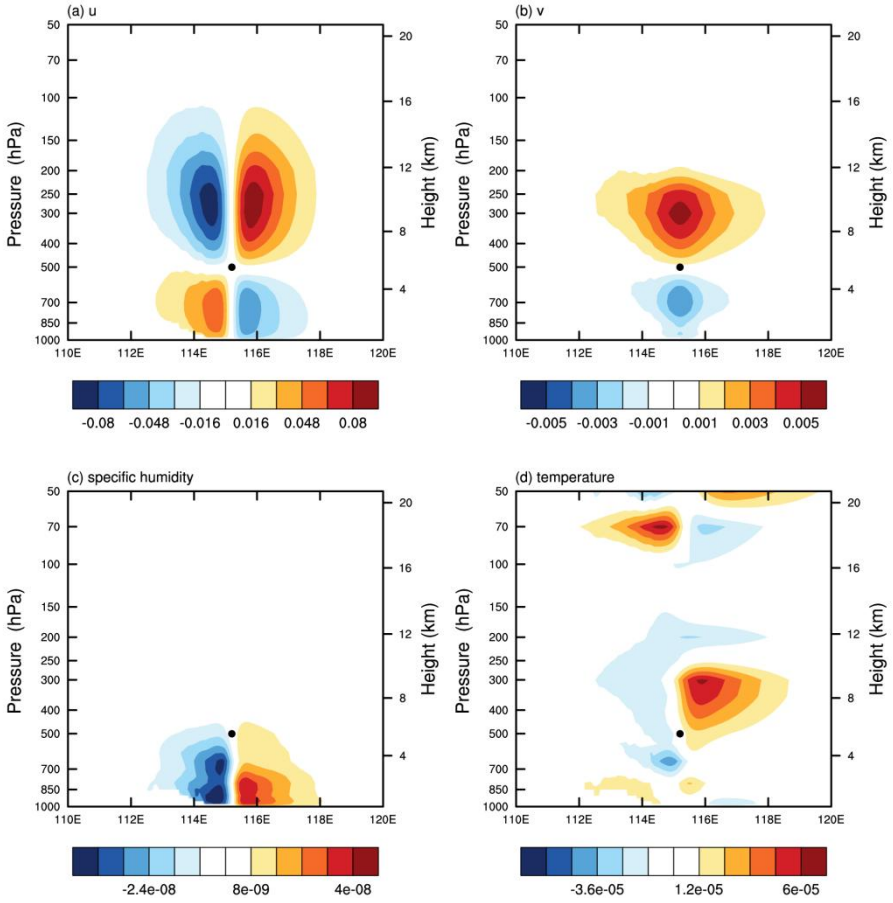

Figure 2: The analysis increments of (a) zonal wind u, (b) meridional wind v (unit: m s^{-1}), (c) specific humidity (unit: kg kg^{-1}), and (d) temperature (unit: K) in a vertical cross-section at 38.0 °N at 1500 UTC on July 4, 2020, for the single observation experiment. The solid black dot in the figure represents the location of the single observation.

4 Validation

In this section, a continuous run is conducted from July 1 to 10, 2020, to evaluate the influence of assimilating w observations on convective precipitation forecasting. Especially, the case that took place on July 9, 2020, from the batch experiments is utilized to have a further study. Additionally, The pseudo-w observations used in this study are derived from radar reflectivity. Notably, the assimilation experiment's scope can be extended to encompass w that is observed or retrieved from alternative sources.

The radar data employed to derive pseudo-observations of w are sourced from the China Next-Generation Weather Radar (CINRAD) network and subjected to quality control procedures. Radar reflectivity serves as an indicator of convection

intensity, while w determines the vigor of convection. Radar reflectivity encompasses information about updraft motion, making it suitable for deriving pseudo-observations of w. Given that the vertical profile of w within the convective zone assumes a parabolic shape (Yuter and Houze, 1995; Collois et al., 2013; Schumacher et al., 2015), empirical Eq. (11), as utilized by Liu et al. (2010), can be employed to derive vertical velocities.

$$w = (\alpha \times (Z - Z_0) + \beta) \times e^{-(\lambda \times (H - H_0))^2}, \quad (11)$$

here, α, β, and λ represent coefficients, with α and β set to 0.1 and 0.3 respectively, in accordance with Liu et al. (2010). The coefficient Z_0 (which is 35 dBZ in this study) denotes the minimum reflectance factor value employed for w retrieval. H_0 signifies the height (unit: km) at which the maximum w value is attained, while λ defines the primary distribution range of w in the vertical direction.

The precipitation observations used to evaluate the model forecast performance are sourced from a merged hourly 0.1°×0.1° precipitation grid dataset, combining data from China's automatic stations and the Climate Prediction Center morphing technique (CMORPH) satellite precipitation data.

4.1 The batch experiment

To assess the assimilation impact of w pseudo-observations, a continuous 10-day run spanning from July 1 to July 10, 2020, was conducted. The simulation area corresponds to the operational area of the CMA-MESO model (refer to Fig. 3 (a)), centered at coordinates (35.05° N, 107.5° E). The horizontal grid comprises 2501×1671 grid points with a grid spacing of 0.03° (~3 km). The vertical dimension is represented by 49 levels extending to a model top of 35 km. Initial and lateral boundary conditions are from the National Centers for Environmental Prediction (NCEP) Global Forecast System (GFS) data. The WSM 6-class microphysics scheme (Hong and Lim, 2006), the Dudhia shortwave radiation scheme (Dudhia, 1989), the Rapid Radiative Transfer Model (RRTM) longwave radiation scheme (Mlawer et al., 1997), and the New Medium Range Forecast (NMRF) planetary boundary layer scheme (Han and Pan, 2006) is adopted. Additionally, cumulus parameterization is closed in these simulations.

4.1.1 Experimental design

Two sets of distinct experiments were configured, and an overview of the experimental setup is depicted in Fig. 3 (b). Both the CTRL and DA-W experiments were initialized at 0000 UTC daily from July 1 to July 10, 2020, and run until 1200 UTC each day. The first 3 hours were considered as "spin-up" period. In the CTRL experiments, observations from aircraft measurements, radiosondes, and other sources (for a comprehensive list, refer to Fig. 3 (b)) were assimilated from 0300 to 0600 UTC with a 1-hour assimilation interval (radial velocity observations are available at each analysis time, while other data sources are only available at 0300 and 0600 UTC). The CTRL-1CY experiment indicates assimilation at 0300 UTC only, while the CTRL-2CY experiment represents assimilation at 0300 and 0400 UTC, and so on (the number preceding the

experiment name "CY" represents the assimilation iterations). The DA-W experiments are similar to the CTRL experiments, but include the assimilation of *w* pseudo-observations (*w* pseudo-observations are available at each analysis time).

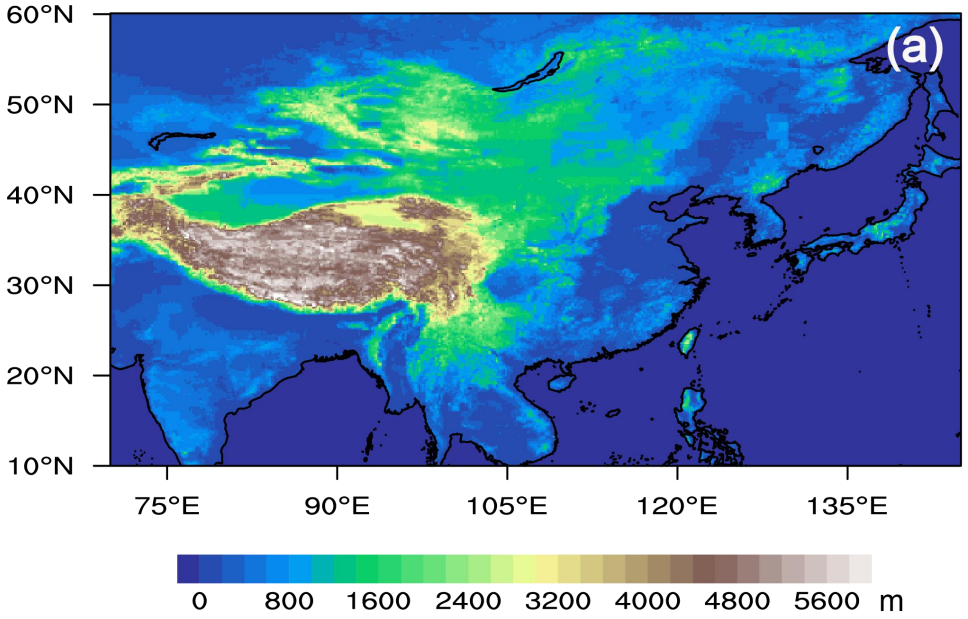

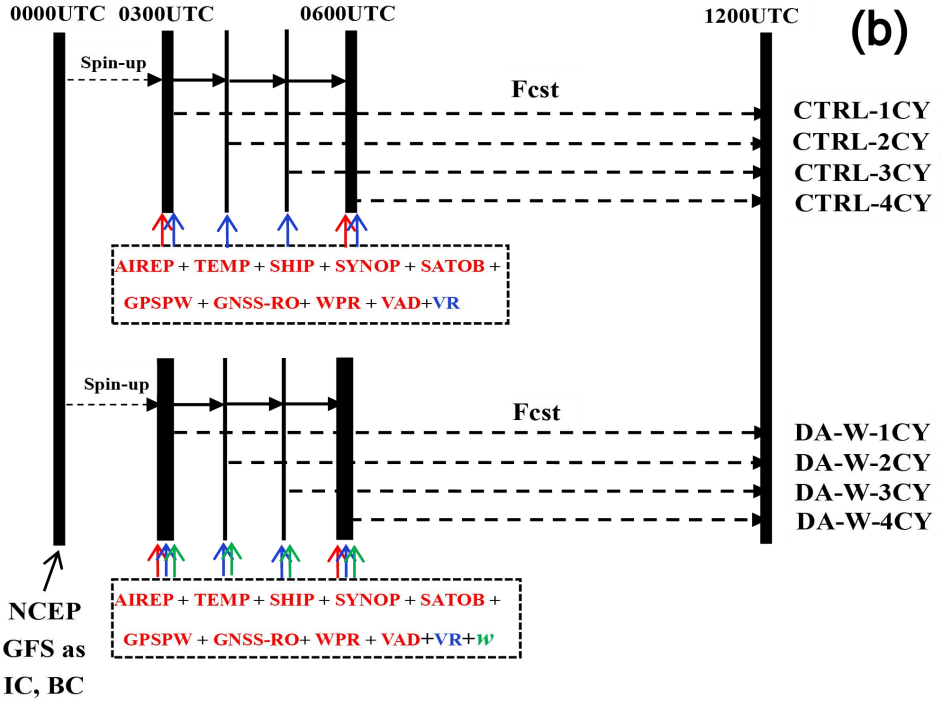

Figure 3: The simulation domain (a) and the numerical experimental scheme (b) for the CTRL and DA-W batch experiments. Both experiments utilize NCEP GFS data as the initial condition (IC) and boundary condition (BC). The abbreviation "Fcst" represents forecast. The assimilated data comprises conventional observations from aircraft measurements (AIREP), radiosondes

(TEMP), ships (SHIP), and ground stations (SYNOP). In addition, cloud-track-wind (SATOB), precipitable water derived from the Global Positioning System (GPSPW), refractivity radio-occultation data from the Global Navigation Satellite System (GNSS-RO), wind profiler radar (WPR), velocity-azimuth display (VAD) wind, and the radar radial velocity (VR) are assimilated. The pseudo-w data is also assimilated for the DA-W experiments.

4.1.2 Results

To statistically evaluate the performance of the CTRL and DA-W experiments for convective precipitation forecasting, the equitable threat score (ETS; Gandin and Murphy, 1992), the neighborhood-based fractions skill score (FSS; Roberts and Lean, 2008), and the bias score (BIAS; Anthes, 1983) are calculated for the forecast hourly accumulated precipitation. Forecasts with higher ETS (close to 1) and FSS (close to 1) and lower BIAS (closer to 1), demonstrate better forecast skills. Figs. 4-6 present the 10-day averaged forecast skills for hourly accumulated precipitation from 0600 UTC to 1200 UTC. For the threshold of 1 mm h^{-1}, it is not always the case that the ETS score improves as the number of assimilation times increases for both CTRL and DA-W experiments. However, with an increase in the scoring threshold, especially for 20 mm h^{-1}, a higher score is generally achieved with more assimilation times, indicating a positive impact of multiple assimilation on the forecast. When comparing the ETS scores of the CTRL and DA-W experiments with the same assimilation times, it can be seen that the DA-W experiment has a neutral or slightly worse effect on the forecast at threshold of 1 mm h^{-1} compared to the CTRL experiment. However, at thresholds of 5 and 20 mm h^{-1}, the DA-W experiment achieves higher scores than the CTRL experiment in most situations, regardless of multiple or single assimilation. Moreover, the experiment with 3 assimilation times (denoted by experiment names ending with "3CY") demonstrate the most significant improvements compared to experiments with other assimilation times.

The FSS scores provide clearer results: for experiments with the same assimilation times in CTRL and DA-W (e.g., DA-W-2CY compared to CTRL-2CY experiment), the DA-W experiment consistently achieves better scores, indicating that the assimilation of w has a better adjustment effect on the forecast of precipitation location. From the BIAS scores, the DA-W experiments have a neutral impact on the forecast compared to the CTRL experiments. In the first 3-hour forecast, the DA-W experiment generally performs worse than the CTRL experiment (with the same assimilation times) for each threshold value, primarily due to producing more false alarms. However, in the latter 3-hour forecast, the DA-W experiment demonstrates better scores compared to the CTRL experiment.

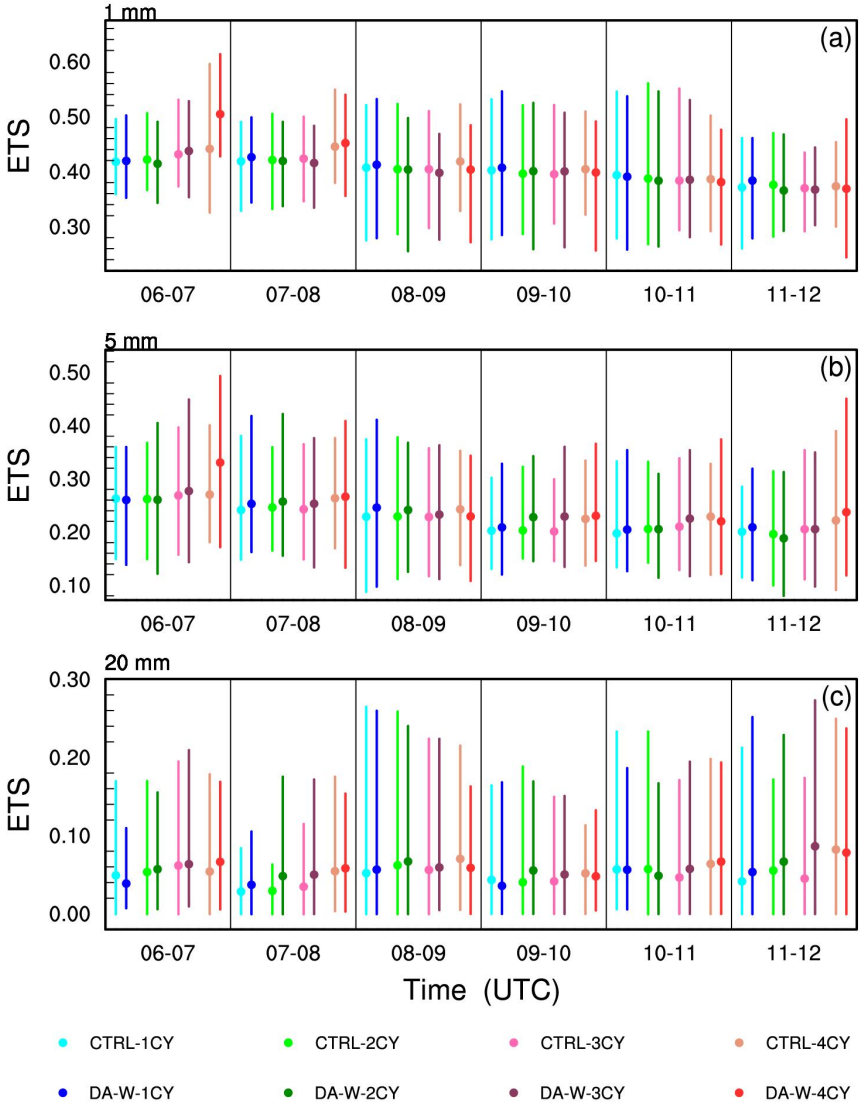

Figure 4: The 10-d (July 1 to July 10, 2020) averaged equitable threat score (ETS; solid dots) of the predicted hourly accumulated precipitation from 0600-1200 UTC of the CTRL and DA-W experiments for thresholds of (a) 1 mm h^{-1}, (b) 5 mm h^{-1}, and (c) 20 mm h^{-1}. The top (bottom) of the line that passes through the solid dot corresponds to the maximum (minimum) ETS value for those 10 days.

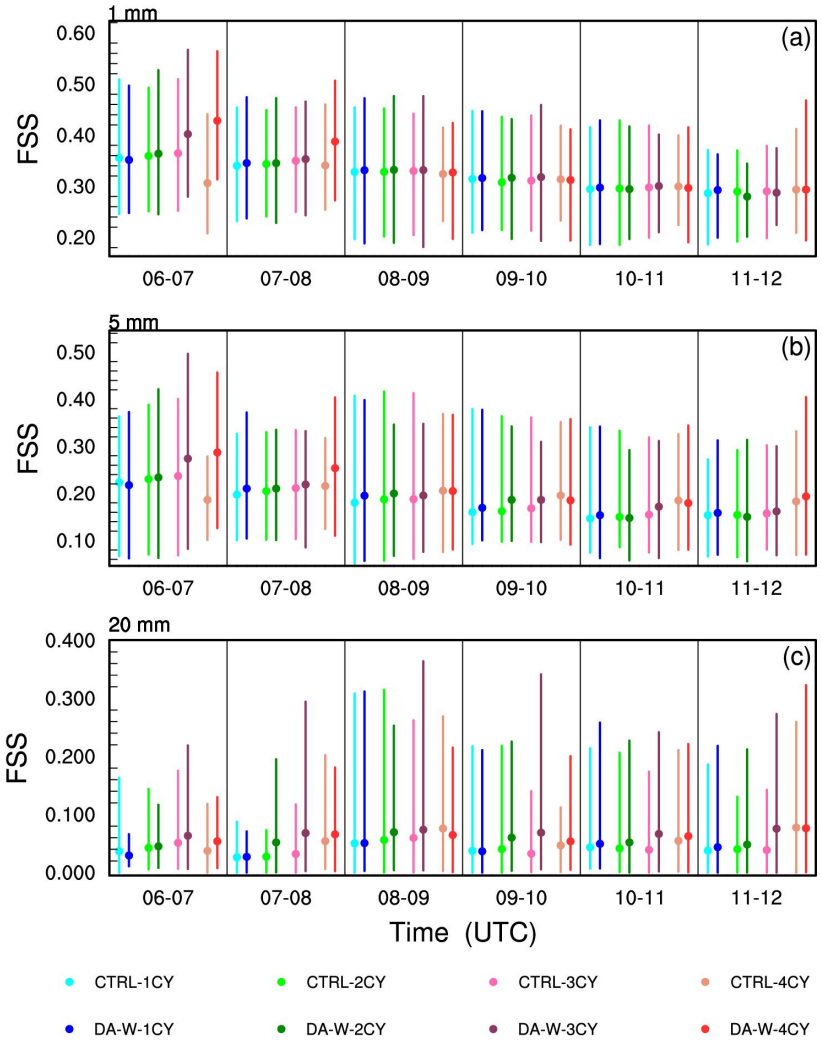

Figure 5: Same as Fig. 4 but for the neighborhood-based fractions skill score (FSS).

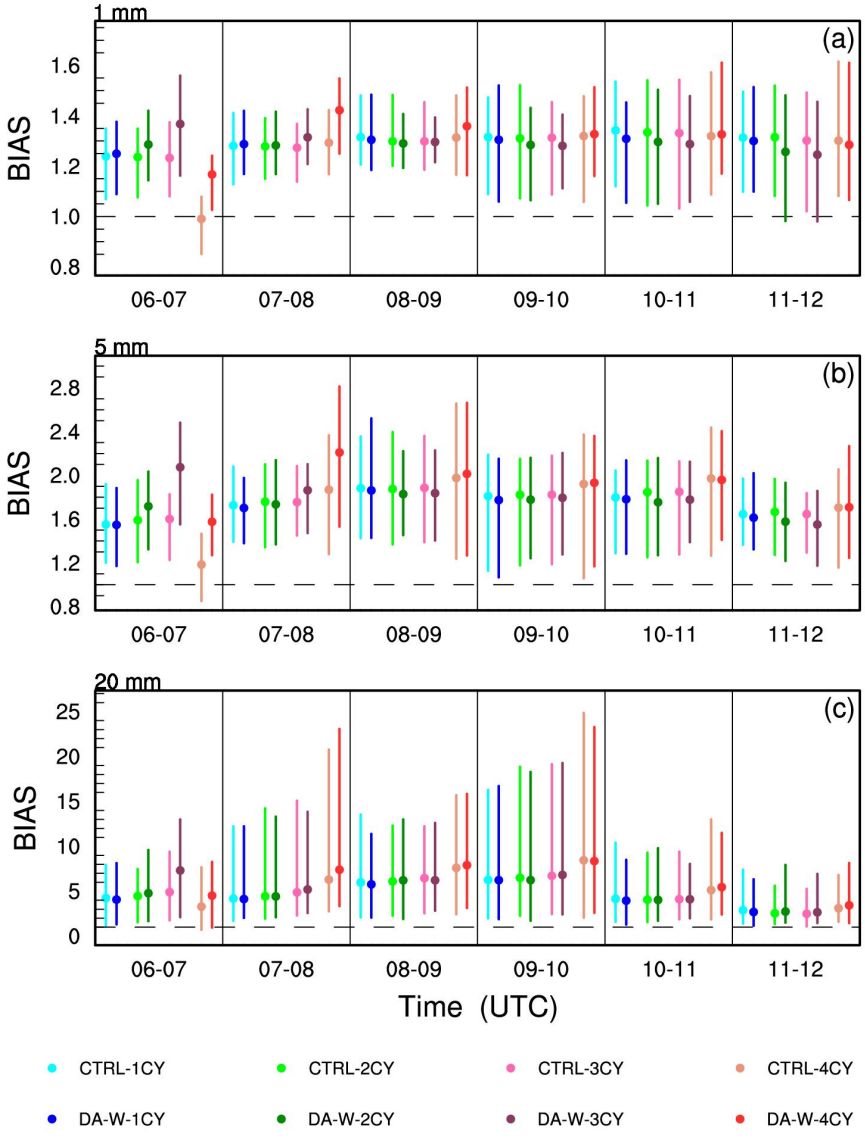

Figure 6: Same as Fig. 4 but for the bias score (BIAS). The black dashed line represents BIAS value equals 1.

4.2 Case study

The case initialized on July 9, 2020 from the batch experiments is chosen to have a further test. Fig. 7 presents the ETS, FSS, and BIAS scores for different thresholds. In both the CTRL and DA-W experiments, increasing the assimilation times does not necessarily result in higher ETS scores, particularly for the 1 mm h^{-1} threshold. However, when comparing the CTRL and DA-W experiments with the same assimilation times, the DA-W experiment consistently achieves higher scores. The FSS scores indicate that, except for the period from 0600 to 0700 UTC, the hourly accumulated precipitation exhibits higher

scores with more assimilation times, and the DA-W experiment consistently outperforms the CTRL experiment. Regarding the BIAS scores, the DA-W experiment has a neutral effect on the forecast compared to the CTRL experiment.

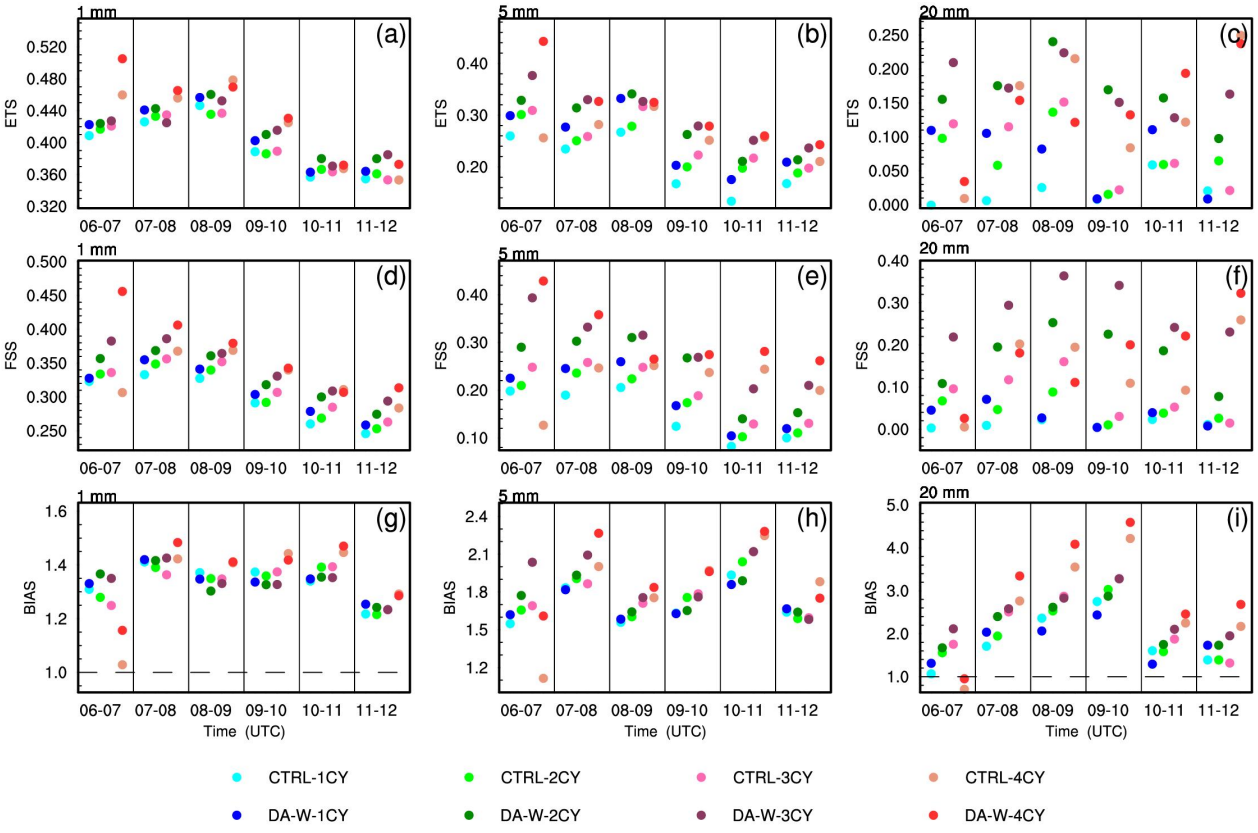

Figure 7: The equitable threat score (ETS; (a)–(c)), the neighborhood-based fractions skill score (FSS; (d)–(f)), and the bias score (BIAS; (g)–(i)) for the predicted hourly accumulated precipitation of the CTRL and DA-W experiments (the black dashed lines in (g) and (i) represent BIAS value equals 1). The analysis focuses on thresholds of 1 mm h^{-1}, 5 mm h^{-1}, and 20 mm h^{-1} for the case initialized at 0000 UTC July 9, 2020.

Fig. 8 displays the 6-hour accumulated precipitation of the CTRL-4CY and DA-W-4CY experiments, with the majority of precipitation occurring in Jiangxi Province. The heavy precipitation center exhibits a maximum 6-hour accumulated precipitation exceeding 100 mm. The CTRL-4CY experiment successfully captures the forecast location of this heavy rainfall area, although the overall precipitation intensity is low. In contrast, the DA-W-4CY experiment performs better in forecasting the intensity of heavy precipitation.

In Fig. 8(a), line A-B represents the observed main precipitation belt. Fig. 9 shows the sections along line A-B for the CTRL-4CY and DA-W-4CY experiments at 0700 UTC on July 9, 2020. The DA-W-4CY experiment effectively enhances the w values across the entire model layers, resulting in a negative water vapor increment below the model's 850 hPa compared to the CTRL-4CY experiment. Simultaneously, positive increments of water vapor are observed in the middle and upper layers of the model.

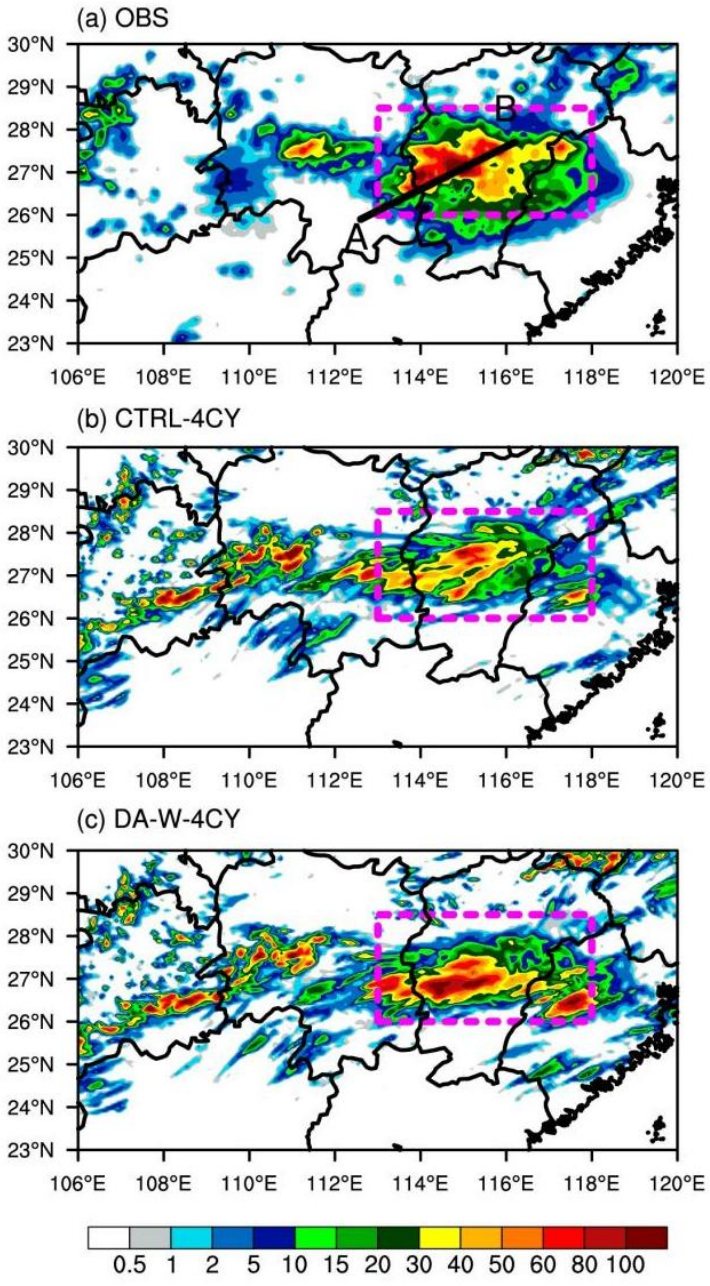

Figure 8: The 6-hour (0600-1200 UTC) accumulated precipitation (units: mm) on July 9, 2020 for (a) observations (OBS), (b) CTRL-4CY, and (c) DA-W-4CY experiments. The areas enclosed by dotted purple lines indicate regions with observed strong rainfall.

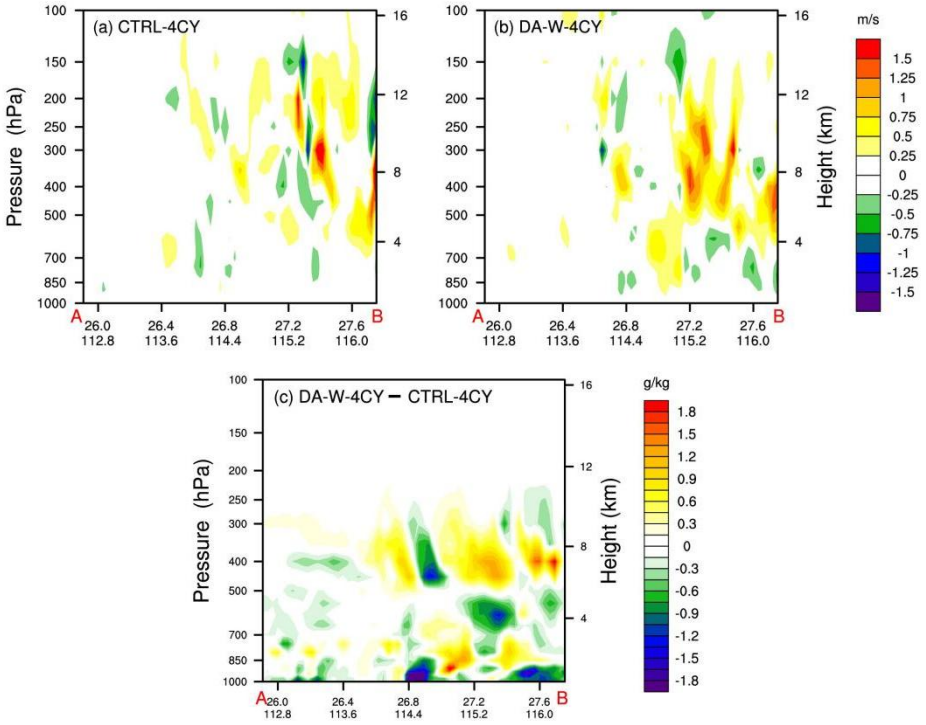

Figure 9: Cross sections of the w (units: m s^{-1}) at 0700 UTC on July 9, 2020, along line A–B in Fig. 8 (a) for the (a) CTRL-4CY and (b) DA-W-4CY experiments. (c) represents the difference in water vapor between the CTRL-4CY and DA-W-4CY experiments (units: g kg-1).

5 Conclusions and discussion

Dynamical processes, especially vertical air motions, play a crucial role in convective precipitation forecasts as they contribute to the development of clouds and precipitation. In this study, a 3D-Var data assimilation scheme for w, based on the adiabatic Richardson equation, is developed within the high-resolution (3 km) CMA-MESO model. The CMA-MESO 3D-Var system employs the horizontal wind components u and v as momentum control variables. The observation operator for w establishes the relationship between w and u, v, as well as Π (dimensionless air pressure). This allows the u and v fields to be updated directly by assimilating w observations. The results of the single observation test indicate a reasonable distribution of horizontal wind increments. Specifically, horizontal wind convergence (resulting from assimilating a positive value of w) is observed at the lower model level (~850 hPa), while horizontal wind divergence tends to occur at the higher model level (~400 hPa). These adjustments effectively contribute to the establishment or reinforcement of convection in these areas.

The impact of assimilating pseudo-observations of w on forecasts is then investigated through the study of a continuous 10-day run and an individual case within it. The pseudo-w observations are derived using the empirical relationship between radar reflectivity factor and w. It should be noted that the w assimilation scheme established in this study is also applicable

to other sources of w. Two sets of experiments were configured, including control (CTRL) experiments with different assimilation iterations and assimilation (DA-W) experiments with different assimilation iterations. Both sets of experiments assimilated aircraft measurements, radiosondes, and other observations (for a comprehensive list, refer to Fig. 3 (b)) at 1-hour intervals during a 3-hour data assimilation period. In addition, the pseudo-w observations are also assimilated in DA-W experiments. The DA-W experiment achieves better higher FSS scores than the CTRL experiment (with the same assimilation times), indicating an improved positional forecast accuracy of precipitation. As for the ETS skills, the DA-W experiment demonstrates enhanced performance than the CTRL experiment at higher thresholds (5 and 20 mm h^{-1}). However, the DA-W experiments tend to generate some spurious precipitation, resulting in inconsistent improvements in BIAS compared to the CTRL experiments. The individual case study indicates that the DA-W experiment contributes to enhancing upward motion in convective regions, resulting in improved forecasts of heavy precipitation that are closer to observations.

Our study has successfully achieved the direct assimilation of w within the current CMA-MESO 3D-Var system, yielding promising preliminary results. However, there are certain limitations that cannot be overlooked and require further attention. For instance: 1) The current approach does not take into account the cross correlation between different control variables of the matrix $\boldsymbol{B}$. The adjustments in temperature and humidity increments are achieved by weak physical constraints. However, the analysis field is significantly affected by the matrix $\boldsymbol{B}$ (Navon et al., 2005). 2) The pseudo-observations of w used in this study are derived from radar reflectivity. However, certain instruments, such as wind profilers, are capable of acquiring w observations. It is valuable to conduct further testing to assess the impact of assimilating these w observations on the forecast. 3) Radar reflectivity observations have traditionally been employed to initialize the moisture field and hydrometeors of regional models (e.g., Albers et al. 1996; Sun and Crook, 1997; Hu et al., 2006; Wang et al., 2013; Lai et al., 2019; Liu et al., 2022), the benefits of assimilating high-resolution radar data might diminish due to inconsistencies in dynamic information. It is imperative to concurrently update dynamical variables in order to maintain a balanced initial field. Our approach could potentially address this issue, given that direct assimilation of w observations is possible. As the CMA-MESO model progresses in incorporating radar reflectivity factor assimilation, the combined assimilation of water vapor, hydrometeors, and w warrants further exploration.

Code availability

The CMA-MESO v5.0 source code is provided by the Chinese Meteorological Administration and cannot be publicly available due to the copyright license requirement from the China Meteorological Administration Earth System Modeling and Prediction Centre (CEMC). If someone wishes to acquire the code to reproduce the study, please contact the operational management department of the CEMC via email (sunqin@cma.gov.cn) or phone (+86-10-58994128). The code of the observation operator, the tangent linear of the observation operator, and the adjoint operator for w is available at https://doi.org/10.5281/zenodo.10073822.

Data availability

The model outputs from the "Single-point observation experiment" and "Case study" sections, along with the processed data from the "The batch experiment" section of the paper, are available at https://doi.org/10.5281/zenodo.10867909. The NCEP GFS data used are available at https://rda.ucar.edu/datasets/ds084.1/. The raw Doppler radar and precipitation observations are provided by the Chinese Meteorological Administration and can be obtained via request from http://www.cma.gov.cn/en2014/.

Author Contributions

Yi Yang conceived the idea and designed the research. Hong Li performed the research and wrote the first draft of the manuscript. All authors discussed the results and contributed to writing and revisions.

Conflict of interest

The authors declare no conflicts of interest or competing financial interests.

Acknowledgments

The authors gratefully acknowledge the CEMC for providing the source code of CMA-MESO v5.0. Additionally, the authors appreciate the NCEP for providing the GFS data and the Chinese Meteorological Administration for providing the radar and precipitation data. Furthermore, special thanks to the Supercomputing Center of Lanzhou University for computational support.

Financial support

This study was jointly supported by the Youth Science and Technology Foundation Program of Gansu Province (23JRRA1327), the National Natural Science Foundation of China (42205050), and the Gansu Provincial Association of Science and Technology Innovation Drive Promotion Project (GXH20230817-7).

References

Albers, S. C., McGinley, J. A., Birkenheuer, D. A., and Smart, J. R.: The local analysis and prediction system (LAPS): Analysis of clouds, precipitation and temperature, Wea. Forecasting, 11, 273–287, doi:10.1175/1520-0434(1996)011<0273:TLAAPS>2.0.CO;2, 1996.

Anderson, N. F., Grainger, C. A., and Stith, J. L.: Characteristics of strong updrafts in precipitation systems over the central tropical Pacific Ocean and in the Amazon, J. Appl. Meteorol., 44, 731–738, doi:10.1175/JAM2231.1, 2005.

Anthes, R. A.: Regional Models of the Atmosphere in Middle Latitudes, Mon. Wea. Rev., 111(6), 1306–1335, doi:10.1175/1520-0493(1983)111<1306:rmotai>2.0.co;2, 1983.

Bellamy, J. C.: Objective calculations of divergence, vertical velocity and vorticity, Bull. Amer. Meteor. Soc., 30, 45–49, 1949.

Chen, Z., Sun, J., Qie, X., Zhang, Y., Ying, Z., Xiao, X., and Cao, D.: A method to update model kinematic states by assimilating satellite-observed total lightning data to improve convective analysis and forecasting, J. Geophys. Res. Atmos., 125(22), 1–26, doi:10.1029/2020jd033330, 2020.

Cifelli, R., Rutledge, S. A., Boccippio, D. J., and Matejka, T.: Horizontal Divergence and Vertical velocity Retrieval from Doppler Radar and Wind Profiler observations, J. Atmos. Ocean. Tech., 13, 948–966, doi:10.1175/1520-0426(1996)013<0948:HDAVVR>2.0.CO;2, 1996.

Collis, S., Protat, A., May, P. T., and Williams, C.: Statistics of storm updraft velocities from TWP-ICE including verification with profiling measurements, J. Appl. Meteorol. Clim., 52, 1909–1922, doi:10.1175/JAMC-D-12-0230.1, 2013.

Courtier, P., Thepaut, J.-N., and Hollingsworth, A.: A strategy for operational implementation of 4D-Var, using an incremental approach, Q. J. R. Meteorol. Soc., 120, 1367–1387, doi:10.1002/qj.49712051912, 1994.

Donner, L. J., Seman, C. J., Hemler, R. S., and Fan, S.: A Cumulus Parameterization Including Mass Fluxes, Convective Vertical Velocities, and Mesoscale Effects: Thermodynamic and Hydrological Aspects in a General Circulation Model, J. Atmos. Sci., 14, 3444–3463, doi:10.1175/1520-0442(2001)014<3444:ACPIMF>2.0.CO;2, 2001.

Dudhia, J.: Numerical study of convection observed during the winter monsoon experiment using a mesoscale two-dimensional model, J. Atmos. Sci. 46(20), 3077–3107, doi:10.1175/1520-0469(1989)046<3077:nsocod>2.0.co;2, 1989.

Gal-Chen, T. J. and Somerville, R. C.: On the use of a coordinate transformation for the resolution of the Navier-Stokes equation, J. Comput. Phys., 17, 209–228, doi:10.1016/0021-9991(75)90037-6, 1975.

Gan, R., Yang, Y., Qiu, X., Wang, R., Qiu, X., and Zhu, L.: Assimilation of the maximum vertical velocity converted from total lightning data through the EnSRF method, J. Geophys. Res. Atmos., 126, e2020JD034300, doi:10.1029/2020JD034300, 2021.

Gan, R., Yang, Y., Qiu, X., Liu, P., Wang, X., and Gu, K.: A scheme to suppress spurious convection by assimilating the "zero" column maximum vertical velocity, J. Geophys. Res. Atmos., 127, e2021JD035536, doi:10.1029/2021JD03553, 2022.

Gandin, L. S. and Murphy, A. H.: Equitable skill scores for categorical forecasts, Mon. Wea. Rev., 120, 361–370, doi:10.1175/1520-0493(1992)120<0361:ESSFCF>2.0.CO;2, 1992.

Giangrande, S. E., Collis, S., Straka, J., Protat, A., Williams, C., and Krueger, S.: A Summary of Convective-Core Vertical Velocity Properties Using ARM UHF Wind Profilers in Oklahoma, J. Appl. Meteorol. Clim., 52(10), 2278–2295, doi:10.1175/jamc-d-12-0185.1, 2013.

Gustafsson, N. and Coauthors: Survey of data assimilation methods for convective-scale numerical weather prediction at operational centers, Quart. J. Roy. Meteor. Soc., 144, 1218–1256, doi:10.1002/qj.3179, 2018.

Han, J. and Pan, H.-L.: Sensitivity of Hurricane Intensity Forecast to Convective Momentum Transport Parameterization, Mon. Wea. Rev., 134(2), 664–674. doi:10.1175/mwr3090.1, 2006.

Heymsfield, G. M., Tian, L., Heymsfield, A. J., Li, L., and Guimond, S.: Characteristics of deep tropical and subtropical convection from nadir-viewing high-altitude airborne Doppler radar, J. Atmos. Sci., 67, 285–308, doi:10.1175/2009JAS3132.1, 2010.

Hong, S.-Y. and Lim, J.-O. J.: The WRF single-moment 6-class microphysics scheme (WSM6), J. Korean Meteor. Sci., 42, 129–151, 2006.

Houze, R. A. Jr. and Betts, A. K.: Convection in GATE, Rev. Geophys., 19, 541–576, doi:10.1029/RG019i004p00541, 1981.

Hu, M., Xue, M., and Brewster, K.: 3DVAR and cloud analysis with WSR-88D Level-II data for the prediction of the Fort Worth tornadic thunderstorms. Part I: Cloud analysis and its impact, Mon. Weather Rev., 134, 675–698, doi:10.1175/MWR3092.1, 2006.

Lai, A., Gao, J., Koch, S. E., Wang, Y., Pan, S., Fierro, A. O., Cui, C., and Min, J.: Assimilation of radar radial velocity, reflectivity, and pseudowater vapor for convective-scale NWP in a variational framework, Mon. Weather Rev., 147, 2877–2900, doi:10.1175/MWR-D-18-0403.1, 2019.

Lang, S., Tao, W.-K., Cifelli, R., Olson, W., Halverson, J., Rutledge, S., and Simpson, J.: Improving simulations of convective Systems from TRMM LBA: Easterly and Westerly Regimes, J. Atmos. Sci., 64, 1141–1164, doi:10.1175/JAS3879.1, 2007.

Lee, J. L., Kuo, Y.-H., and MacDonald, A. E.: The vorticity method: Extension to mesoscale vertical velocity and validation for tropical storms, Quart. J. Roy. Meteor. Soc., 129, 1029–1050, doi:10.1256/qj.01.219, 2003.

Lee, J. L., Lee, W. C., and MacDonald, A. E.: Estimating vertical velocity and radial flow from Doppler radar observations of tropical cyclones, Quart. J. Roy. Meteor. Soc., 132, 125–145, doi:10.1256/qj.04.77, 2006.

LeMone, M. A. and Zipser, E. J.: Cumulonimbus vertical velocity events in GATE. Part I: Diameter, intensity and mass flux, J. Atmos. Sci., 37, 2444–2457, doi:10.1175/1520-0469(1980)037<2444:CVVEIG>2.0.CO;2, 1980.

Liu, H. Y., Xue, J. S., Gu, J. F., and Xu, H. M.: GRAPES-3DVAR radar data assimilation and numerical simulation experiments with a torrential rain case, Acta Meteorological Sinica, 68(6), 779–789, 2010. (in Chinese)

Liu, P., Yang, Z. D., Wang, X. S., Qiu, X. B., and Yang, Y.: Assimilation of the pseudo-water vapor derived from extrapolated radar reflectivity to improve the forecasts of convective events, Atmos. Res., 279(3):106386, doi:10.1016/j.atmosres.2022.106386, 2022.

Liu, S., Qiu, C., Xu, Q., Zhang, P., Gao, J., and Shao, A.: An improved method for Doppler wind and thermodynamic retrievals, Adv. Atmos. Sci., 22, 90–102, doi:10.1007/BF02930872, 2005.

May, P. T., Mather, J. H., Vaughan, G., Jakob, C., McFarquhar, G. M., Bower, K. N., and Mace, G. G.: The tropical warm pool international cloud experiment, Bull. Amer. Meteor. Soc., 89, 629–645, doi:10.1175/BAMS-89-5-629, 2008.

Mlawer, E. J., Taubman, S. J., Brown, P. D., Iacono, M. J., and Clough, S. A.: Radiative transfer for inhomogeneous atmospheres: RRTM, a validated correlated-k model for the longwave, J. Geophys. Res. Atmos., 102, 16663–16682, doi:10.1029/97JD00237, 1997.

Navon, I. M., Daescu, D. N. and Liu, Z.: The impact of background error on incomplete observations for 4D-Var data assimilation with the FSU GSM, Lect. Notes Comput. Sci., 3515, 837–844, 2005.

Kalnay, E.: Atmospheric Modeling, Data Assimilation, and Predictability, Cambridge University Press, 2002.

Ovchinnikov, M., Giangrande, S., Larson, V. E., Protat, A., and Williams, C. R.: Dependence of vertical alignment of cloud and precipitation properties on their effective fall speeds, J. Geophys. Res. Atmos., 124(4), 2079–2093, doi:10.1029/2018JD029346, 2019.

Panosetti, D., Schlemmer, L., and Schär, C.: Bulk and structural convergence at convection-resolving scales in real-case simulations of summertime moist convection over land, Quart. J. Roy. Meteor. Soc., 145, 1427–1443, doi:10.1002/qj.3502, 2019.

Price, C. and Rind, D.: A simple lightning parameterization for calculating global lightning distributions, J. Geophys. Res. Atmos., 97, 9919–9933, doi:10.1029/92JD00719, 1992.

Richardson, L. F.: Weather Prediction by Numerical Process, Cambridge University Press, 236 pp, 1922.

Roberts, N.M. and Lean, H.W.: Scale-selective verification of rainfall accumulations from high-resolution forecasts of convective events, Mon.Wea. Rev., 136, 78–97, doi:10.1175/2007MWR2123.1, 2008.

Rodts, S. M. A., Duynkerke, P. G., and Jonker, H. J. J.: Size distributions and dynamical properties of shallow cumulus clouds from aircraft observations and satellite data, J. Atmos. Sci., 60, 1895–1912, doi:10.1175/1520-0469(2003)060<1895:SDADPO>2.0.CO;2, 2003.

Schumacher, C., Stevenson, S. N. and Williams, C. R.: Vertical motions of the tropical convective cloud spectrum over Darwin, Australia, Q. J. Roy. Meteor. Soc., 141, 2277–2288, doi:10.1002/qj.2520, 2015.

Shen, X. S., Wang, J. J., Li, Z. C., Chen, D. H., and Gong, J, D.: Research and operational development of numerical weather prediction in China, J. Meteor. Res., 34(4), 675–698, doi:10.1007/s13351-020-9847-6, 2020.

Sun, J. and Crook, N. A.: Dynamical and microphysical retrieval from Doppler radar observations using a cloud model and its adjoint. Part I: Model development and simulated data experiments, J. Atmos. Sci., 54, 1642–1661, doi:10.1175/1520-0469(1997)054<1642:DAMRFD>2.0.CO;2, 1997.

Tao, W.-K., Iguchi, T., Lang, S., Li, X., Mohr, K., Matsui, T., et al.: Relating vertical velocity and cloud/precipitation properties: A numerical cloud ensemble modeling study of tropical convection, J. Adv. Model. Earth Syst., 14, e2021MS002677, doi:10.1029/2021MS002677, 2022.

Tarry, D. R., Ruiz, S., Johnston, T., Poulain, P.-M., Özgökmen, T., Centurioni, L. R., et al.: Drifter observations reveal intense vertical velocity in a surface ocean front, Geophys. Res. Lett., 49, e2022GL098969, doi:10.1029/2022GL098969, 2022.

Wang, H., Chen, D., Yin, J., Xu, D., Dai, G., and Chen, L.: An improvement of convective precipitation nowcasting through lightning data dynamic nudging in a cloud-resolving scale forecasting system, Atmos. Res., 242, 1–11, doi:10.1016/j.atmosres.2020.104994, 2020.

Wang, H., Sun, J., Fan, S., and Huang, X.-Y.: Indirect assimilation of radar reflectivity with WRF 3D-Var and its impact on prediction of four summertime convective events, J. Appl. Meteorol. Climatol., 52, 889–902, doi:10.1175/JAMC-D-12-0120.1, 2013.

Williams, C. R.: Vertical air motion retrieved from dual-frequency profiler observations, J. Atmos. Ocean. Tech., 29(10), 1471–1480, doi:10.1175/jtech-d-11-00176.1, 2012.

Xiao, X., Sun, J., Qie, X., Ying, Z., Ji, L., Chen, M., and Zhang, L.: Lightning data assimilation scheme in a 4DVAR system and its impact on very short-term convective forecasting, Mon. Weather Rev., 149(2), 353–373, doi:10.1175/mwr-d-19-0396.1, 2021.

Yuter, S. E. and Houze, R. A.: Three-dimensional kinematic and microphysical evolution of Florida cumulonimbus: Part II. Frequency distribution of vertical velocity, reflectivity, and the differential reflectivity, Mon. Weather Rev., 123, 1941–1963, doi:10.1175/1520-0493(1995)123<1941:TDKAME>2.0.CO;2, 1995.